ELSEVIER

Journal of Fluids and Structures 21 (2005) 395–412

JOURNAL OF FLUIDS AND STRUCTURES

www.elsevier.com/locate/jfs

Dynamics of an oscillating bubble near a floating structure

E. Klaseboer[a], B.C. Khoo[b,c,*], K.C. Hung[a]

[a]*Institute of High Performance Computing, 1 Science Park Road #01-01, The Capricorn, Singapore 117528, Singapore*
[b]*Department of Mechanical Engineering, National University of Singapore, 10 Kent Ridge Crescent, Singapore 119260, Singapore*
[c]*MIT Alliance, 4 Engineering Drive 3, Singapore 117576, Singapore*

Received 25 August 2004; accepted 12 August 2005
Available online 5 October 2005

Abstract

A method to describe the behaviour of an oscillating bubble near a free surface and a floating structure is described in this article using the boundary integral method. The free surface is modelled using a negative image of the bubble (and the submerged part of the structure) pertinent to a reasonably deep underwater explosion where the free surface remains almost flat. This approach obviates the need to model the free surface separately. Several examples are provided to show the combined complex interaction of the attraction of the bubble towards the solid surface, the repulsion by the free surface and the influence of gravity.

Keywords: Boundary integral method; Underwater explosion; Free surface; Ship; Bubble dynamics

1. Introduction

Bubbles have intrigued mankind for centuries and many problems relating to bubble dynamics remain unsolved or are not yet well understood up to the present day (Prosperetti, 2004). Oscillating bubbles can be found in many fields of engineering ranging from cavitation on ship propellers, underwater explosions to even micro bubbles in medical treatments. Initially, spherical symmetrical bubble oscillations were investigated, see for example Rayleigh (1917). Much later, it was discovered that in many cases the bubble assumes a nonspherical symmetric configuration during the collapse phase. Several experimental and numerical studies have clearly shown that if a bubble oscillates near a solid surface (if buoyancy can be neglected and in a stationary ambient flow), a jet will be formed in the bubble; see for example Naude and Ellis (1961), Benjamin and Ellis (1966), Plesset and Chapman (1971), Blake et al. (1986), Chan et al. (2000) or Zhang et al. (2001). This jet originates from the side that is facing away from the solid and traverses the bubble with great speed until it impacts on the opposite bubble wall. The bubble will be slightly repelled from the solid surface during its expansion phase and strongly attracted towards it during its collapse phase.

On the other hand, if a bubble oscillates near a free surface, again under the assumption of zero buoyancy and no ambient flow, a jet directed away from this surface can be formed during the collapse phase of the bubble; see for example Chahine (1977), Blake and Gibson (1981, 1987), Longuet-Higgins (1983), Blake et al. (1987) or Wang et al. (1996a, b). The bubble as a whole will be repulsed by the free surface. Even in the absence of any surface in the vicinity

*Corresponding author. Department of Mechanical Engineering, National University of Singapore, 10 Kent Ridge Crescent, Singapore 119260, Singapore. Tel.: +65 68742889; fax: +65 67791459.
E-mail address: mpekbc@nus.edu.sg (B.C. Khoo).

0889-9746/$ - see front matter
doi:10.1016/j.jfluidstructs.2005.08.006

of the bubble, a jet still can be formed in large bubbles due to the effect of gravity. This jet will always be directed upwards (in opposite direction to the gravity vector); see Wang et al. (2003) for an example. For an overview of the phenomena discussed above, see Blake and Gibson (1987). To the best knowledge of the authors, the dynamics of a bubble depicting the combined effects of a free surface, solid surface and gravity have not yet been reported in the literature. This situation can typically occur when an underwater explosion occurs near a floating ship. In this article a method based on the boundary integral method (BIM) will be introduced and broadly described. For greater details or a review on the use of the BIM in bubble dynamics the reader is referred to: Taib (1985), Blake et al. (1986, 1987), Harris (1992), Chahine (1994), Zhang et al. (1998, 2001) or Wang et al. (2003) to name a few. In this work, the proposed modification of the BIM method makes use of the fact that the free surface can act as a negative mirror if the free surface remains relatively flat during the underwater explosion. The above assumption is valid for a reasonably deep submerged explosion bubble.

The outline of the paper is as follows. In Section 2 the basic equations that govern the dynamics of the bubble will be described. Some examples are given of bubbles oscillating near free surfaces. Special emphasis is placed on the second oscillating phase, which has often been ignored in previous works. Also the effects of gravity are investigated in this section. In Section 3 the theoretical framework for the proposed 'negative mirror' method is given. A comparison is given with an existing axial symmetrically code which produces nearly identical results. In Sections 2 and 3, no floating structure has been introduced yet. In Section 4 the dynamics of (large) bubbles near a free surface and a (fixed) floating structure are investigated. Several examples showing very complex bubble behaviour can be observed under certain circumstances.

2. Basic equations

2.1. Fluid dynamics equations

Consider an incompressible fluid with an oscillating bubble with its centre at an initial distance H away from a free surface. The free surface is initially quiescent (corresponding to a value of the z co-ordinate of 0.0, with z pointing into the water). We shall further assume that the fluid is irrotational and that viscous effects can be neglected (since the flow is at high Reynolds number and is essentially inertia driven). As such, a velocity potential Φ can be introduced that obeys the following equation for the velocity vector: $\boldsymbol{v} = \nabla\Phi$ (bold variable here and elsewhere are taken as vectors in this work). This equation together with the continuity equation $\nabla \cdot \boldsymbol{v} = 0$ leads to the Laplace equation which is valid anywhere in the fluid

$$\nabla^2\Phi = 0. \tag{1}$$

The Laplace equation is an elliptic equation, hence implying that the solution is known anywhere in the fluid domain, if either the potential Φ (Dirichlet condition) or the normal velocity $U\left(= \partial\Phi/\partial n\right)$ (Neumann condition) is given on the boundaries of the problem. The time-dependent Bernoulli equation, which drives the problem of interest, can be applied anywhere in the fluid

$$p = p_{\mathrm{ATM}} - \rho\frac{D\Phi}{Dt} + \frac{1}{2}\rho|\boldsymbol{v}|^2 + \rho g z, \tag{2}$$

where p is the pressure, p_{ATM} is the atmospheric pressure, ρ is the density of the fluid, g is the gravity acceleration and z is the vertical coordinate in the direction of the gravity vector. The material derivative D/Dt with respect to velocity $\boldsymbol{v}$ is used in (2) and is defined as $Dx/Dt = \partial x/\partial t + \boldsymbol{v} \cdot \nabla x$. At the free interface the pressure is equal to the atmospheric pressure (if surface tension effects are neglected, which can be done for the large bubbles under consideration), thus

$$\rho\frac{D\Phi}{Dt} = \frac{1}{2}\rho|\boldsymbol{v}|^2 + \rho g z \quad \text{(on free interface)}. \tag{3}$$

Note that in Section 3 a simplified model will be introduced which replaces Eq. (3). Inside the bubble, the pressure p_g is supposed to be spatially uniform and is governed by the adiabatic formula

$$p_g = p_{g,0}\left(\frac{V_0}{V}\right)^{\gamma}. \tag{4}$$

Here V is the volume of the bubble and $p_{g,0}$ and V_0 are the pressure and volume at the time of inception of the bubble, respectively. The ratio of the specific heats γ equals 1.25 for underwater explosions with TNT, Cole (1948). The value $\gamma = 1.25$ has been chosen throughout this work. Combining (2) and (4) leads to the following equation for the potential

at the bubble surface:

$$\rho\frac{D\Phi}{Dt} = p_{\mathrm{ATM}} - p_{g,0}\left(\frac{V_0}{V}\right)^{\gamma} + \frac{1}{2}\rho|\mathbf{v}|^2 + \rho g z \quad \text{(on bubble surface)}. \tag{5}$$

At $t = 0$ the potential is set to a value of zero at all boundaries (bubble, free surface and solid surface if present)

$$\Phi(t = 0) = 0. \tag{6}$$

The free surface is assumed to be initially flat and quiescent at $z = 0$. The bubble is also assumed to be spherically symmetric with an initial radius R_0 and its centre is located at $z = H$ at $t = 0$. For any structure the following zero normal velocity constraint is applied at all times:

$$\frac{\partial\Phi}{\partial n} = U = 0 \quad \text{(on a structure)}. \tag{7}$$

Eq. (7) implies that the structure is fixed, but it can easily be extended to include moving or deforming structures by setting U to an imposed or evaluated non zero value.

2.2. The explosive

For an explosive, the charge weight (W as expressed in kg) and the depth at which it explodes (H as expressed in m) are generally known. The relationship between these two parameters and the initial radius for the numerical calculations (R_0) and the maximum bubble radius (R_m) will be established now. At the same time an expression for the initial gas pressure inside the bubble just after the explosion $p_{g,0}$ will be obtained. For a TNT-charge, an empirical relationship between W, H and R_m exists [see Cole (1948) or Rungsiyaphornrat et al. (2003)]. This is given as

$$R_m = 3.38\left(\frac{W}{H + 10}\right)^{1/3}. \tag{8}$$

The maximum volume of the bubble will thus be linearly dependent on the charge weight and inversely proportional to the hydrostatic pressure (the factor '10' in (8) originates from the atmospheric pressure). Another empirical relationship for the initial pressure of the explosion products (TNT-explosives) is

$$p_{g,0} = 1.39 \times 10^5\left(\frac{W}{V_0}\right)^{\gamma}. \tag{9}$$

The equation of motion for a spherically symmetric bubble oscillating at a depth H (the so-called Rayleigh–Plesset equation) is

$$p_g - p_{\mathrm{ATM}} - \rho g H = \frac{3}{2}\rho\left[\frac{\mathrm{d}R}{\mathrm{d}t}\right]^2 + \rho R\frac{\mathrm{d}^2R}{\mathrm{d}t^2}. \tag{10}$$

In this equation, surface tension effects, vapour pressure and compressibility of the fluid have been neglected. This equation will be used to obtain the radius of the bubble R_0 at $t = 0$. Eq. (10) can be solved using (4) and the following relationship for the bubble surface velocity can be found

$$\frac{3}{2}\rho\left(\frac{\mathrm{d}R}{\mathrm{d}t}\right)^2 = (p_{\mathrm{ATM}} + \rho g H)\left[-1 + \left(\frac{R_0}{R}\right)^3\right] - \frac{p_{g0}}{\gamma - 1}\left[\left(\frac{R_0}{R}\right)^{3\gamma} - \left(\frac{R_0}{R}\right)^3\right]. \tag{11}$$

This equation can be easily shown to be correct by substituting (11) and its derivative with time back into (10). Note that Eq. (11) is only valid for values of $\gamma \neq 1$. If $\gamma = 1$, the bubble's contents behave as an isothermal gas and another relationship similar to (11) has to be used. At $R = R_0$ the bubble surface velocity is 0, as it is initially at rest. Using the fact that at $R = R_m$ the bubble velocity should also be zero for a spherical bubble, an equation from which R_0 can be solved is obtained with (8) and (9). This is carried out by a root solving procedure for R_0

$$(p_{\mathrm{ATM}} + \rho g H)\left[-1 + \left(\frac{R_0}{R_m}\right)^3\right] = \frac{1.39 \times 10^5}{\gamma - 1}\left(\frac{3W}{4\pi R_0^3}\right)^{\gamma}\left[\left(\frac{R_0}{R_m}\right)^{3\gamma} - \left(\frac{R_0}{R_m}\right)^3\right]. \tag{12}$$

It should be noted that the R_0 obtained here is a purely numerical quantity and, in general, does not relate directly to the initial size of the explosive. The initial gas pressure $p_{g,0}$ can be calculated with (9).

2.3. Dimensionless equations

The foregoing equations can be made dimensionless. The most suitable scaling factor for length is the maximum bubble radius R_m obtained from (8). The reference pressure is taken to be the ambient pressure at the depth H,

$$p_{\mathrm{Ref}} = p_{\mathrm{ATM}} + \rho g H. \tag{13}$$

The other scaling factors for time and potential are chosen to be, respectively, $R_m\sqrt{\rho/p_{\mathrm{Ref}}}$ and $R_m\sqrt{p_{\mathrm{Ref}}/\rho}$. Eq. (3) can now be written in dimensionless form

$$\frac{D\Phi'}{Dt'} = \frac{1}{2}\left|\nabla'\Phi'\right|^2 + \delta z' \quad \text{(on free surface)}. \tag{14}$$

On the bubble surface (5) becomes

$$\frac{D\Phi'}{Dt'} = 1 - \varepsilon\left(\frac{V_0'}{V'}\right)^{\gamma} + \frac{1}{2}\left|\nabla'\Phi'\right|^2 + \delta(z' - H') \quad \text{(on bubble surface)}. \tag{15}$$

The dimensionless parameters introduced above are the strength parameter ε, the buoyancy parameter δ and the depth parameter H':

$$\varepsilon = \frac{p_{g,0}}{p_{\mathrm{Ref}}}, \tag{16}$$

$$\delta = \frac{\rho g R_m}{p_{\mathrm{Ref}}}, \tag{17}$$

$$H' = \frac{H}{R_m}. \tag{18}$$

On the solid surface (if present) the zero normal velocity boundary condition applies, or equivalently

$$U' = 0 \quad \text{(on solid surface)}. \tag{19}$$

Using (17) and (13) and noting that H should not be much smaller than R_m (otherwise the bubble would vent to the surface at an early stage), it can reasonably be assumed that δ takes on a value between 0 and 1. If $\delta\sim 0$, the effects of gravity can be neglected. For underwater explosions, δ has a typical value of about 0.25 and can certainly not be neglected. Eq. (12) can be rewritten in dimensionless form

$$-1 + R_0'^3 = \frac{\varepsilon}{\gamma - 1}\left[R_0'^{3\gamma} - R_0'^3\right]. \tag{20}$$

The parameters ε, $R_0'$and γ are related to each other by (20) and only two of them can be chosen freely. Finally, for the kinematic surface velocity (on the bubble and on the free surface) we have:

$$\frac{Dx'}{Dt'} = \nabla'\Phi'. \tag{21}$$

This equation is used to update the position vectors of the nodes of the bubble at every time step.

2.4. Toroidal bubbles

During the collapse phase of the bubble, usually a liquid jet is created that traverses across the bubble with very high speed. If the liquid jet impacts on the opposite face of the bubble, the fluid domain becomes doubly connected. Numerically, two challenges arise when this happens. First of all, some re-meshing has to be performed in order to connect the fluid of the jet and the fluid on the far side of the bubble. In an axial symmetrical configuration this is quite straightforward [see Blake et al. (1997) or Wang et al. (1996b)], but it can be rather complex for Three-dimensional (3-D) models [see Zhang et al. (2001) for more details on the 'surgical cut' in a 3-D configuration]. Furthermore the jet impact will generate a circulation in the fluid. Zhang and Duncan (1994) have modelled this circulation by introducing a vortex sheet that moves with the fluid. This vortex sheet can become highly distorted as the bubble evolves. A simpler model consists of placing a vortex ring inside the bubble enclosing the jet. The strength of this vortex ring is chosen to be equal to the potential difference of the jet and the opposite bubble surface just before the jet impacts. The potential is now decomposed in to two parts, one corresponding to the circulation of the jet impact (Ψ')

and a remainder (φ'),

$$\Phi' = \Psi' + \varphi' \tag{22}$$

The potential Ψ' exhibits a jump across the vortex ring; the potential φ' is smooth throughout the whole fluid domain. An analytical solution can be found for the velocity field generated by Ψ'. The exact position of the vortex ring does not influence the outcome of the numerical solution, as long as it is not placed too near to the surface of the bubble (to avoid numerical instabilities). For more details the reader is referred to Zhang et al. (2001). The boundary integral equation (as introduced in Section 2.5 or Section 3) is now solved for φ' with associated modifications in (14) and (15). Furthermore, the normal velocity on any solid surface in (19) must be replaced by the negative value of the normal velocity caused by Ψ', in order to keep the total normal velocity equal to zero.

2.5. Boundary integral simulations for axial-symmetrical problems

The solution of the Laplace equation (1) is fully determined by its boundary conditions. This means that, once the boundary conditions are set, the solution is known everywhere (in principle). The boundary element method takes advantage of this principle, by reducing the Laplace equation into an integral equation. The dimension of the problem under consideration will be reduced by one. This greatly reduces the number of grid points needed (one only needs grid points on the boundaries and none inside the fluid domain). It is also easier to follow any moving boundary (such as the bubble's interface or the free surface) using this approach.

Many numerical results concerning the axisymmetrical configuration of an oscillating bubble near a free surface have appeared in previous works. For small bubbles, where gravity can be neglected, Robinson et al. (2001) simulated bubbles at the dimensionless distance of $H' = 0.95$ and 0.56. Wang et al. (1996a) simulated bubbles with a stand off distance of $H' = 1.5$, 1.0, 0.7 and 0.5 (with neglect of gravity). From all these results, it can be concluded that a downwards directed jet is induced during the bubble collapse phase while at the same time a water plume is created at the free surface. The plume height is very sensitive to H'. It was also observed that the oscillation time of a bubble is reduced when compared to the equivalent of a free field bubble. On the other hand, the oscillation time increases for a bubble located near a solid surface as compared to a free field bubble [see Klaseboer and Khoo (2004)]. As we will see later, this is an important consideration for the sequence of events to occur relating to a bubble oscillating near a free surface and a solid surface at the same time. Other experimental results can be found in Blake and Gibson (1981), where very clearly the upwards directed water plume at the free surface and the downwards jet in the bubble can be observed. For all these studies on a single bubble and free surface, attention was not directed on the second expansion phase of the bubble. Therefore, we will investigate two cases where some emphasis will be on this second expansion phase (i.e. the expansion after its initial contraction/collapse phase).

We will do so, by taking into account the effect of buoyancy through the parameter δ, which is nonnegligible in underwater explosions. As observed in several works [for example Wang et al. (1996b)], gravitational effects can take precedence over the dynamics of the bubble and the jet can be directed in the upwards direction, instead of the usual downwards direction. Two cases with the inclusion of gravity effects can be found in Figs. 1 and 2. The parameters are $\varepsilon = 500$ and $H' = 1.1$. The axisymmetrical numerical code of Wang et al. (1996a, b) is employed here. In Fig. 1, δ has a value of 0.25 and in Fig. 2, δ takes on a value twice as large, namely 0.5. A broad comparison of the expansion phases of the bubbles in Figs. 1(a) and 2(a) shows that the results are fairly similar, except that the bubble expands more and cuts across the line $z' = 0$ for the larger $\delta = 0.5$. The collapse phase is, however, completely different for the two cases. For $\delta = 0.0$, the jet in the bubble would be directed downwards (results not shown here). A closer scrutiny of Fig. 1(a) reveals the existence of an upwards and downwards directed jet at the same time. The downwards directed jet is induced by the effect of the free surface, while the upwards directed jet is induced by gravity (gravity in most cases is responsible for a jet directed in the opposite direction of the gravity vector for large oscillating bubbles). These two jets impact on each other slightly below the centre of the bubble at $t' = 1.533$. It is interesting to note the event after the bubble enters its second expansion phase; a ring shaped elevation occurs on the free surface in Fig. 1(b). For an even larger value of δ at 0.5 in Fig. 2(a), the jet inside the bubble is directed upwards. In this case gravity effects completely dominate the dynamics of the bubble. The bubble in Fig. 2(b) moves much faster towards the free surface in its second expansion phase than that in Fig. 1(b). It is highly likely that instabilities will occur at the thin interface between the bubble and the free interface and next lead to the venting phenomenon. This, however, is outside the scope of the current investigations.

In Fig. 3, the plume height as a function of H' is given for several values of δ. The plume height has been taken as the maximum value of the surface along the axis of symmetry during the first expansion and collapse phase. A very sharp rise in the plume height can be observed for values of H' smaller than 1. For values of H' lower than, say 0.75, the observed plume height is larger than the maximum bubble radius (which is 1.0 for this dimensionless figure). The plume height rapidly decreases for increasing values of H'. The influence of gravity (through δ) is observed to be less important, compared to the very sharp rise of the height of the plume as a function of H'.

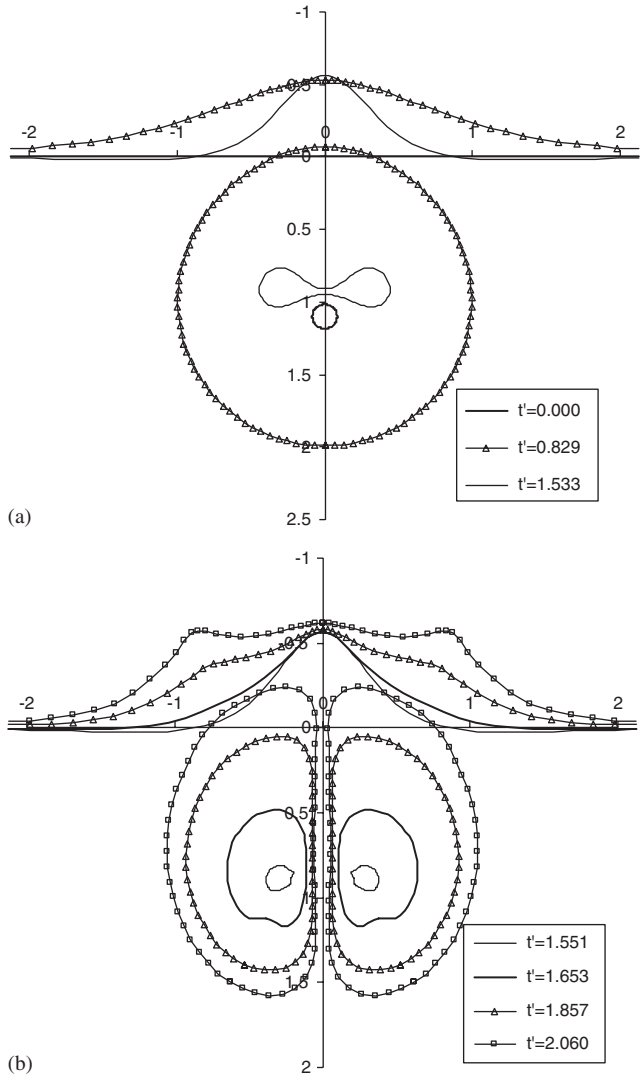

Fig. 1. Axially symmetric simulation of a bubble situated at an initial depth of $H' = 1.1$ with parameters $\varepsilon = 500$ and $\delta = 0.25$. (a) Bubble in its first expansion and collapse phase at $t' = 0.000$, $t' = 0.829$ and $t' = 1.533$. (b) Bubble in its second expansion phase at $t' = 1.551$, $t' = 1.653$, $t' = 1.857$ and $t' = 2.060$.

The two examples of Figs. 1 and 2 are provided to illustrate the complexities of the bubble dynamics and the associated free surface behaviour. These are dependent on the bubble depth H', the strength of the bubble, ε and the buoyancy parameter δ (which takes into account the effects of gravity). In this section, no solid surface was introduced yet; this will be done in the next section.

3. Simplified model using negative mirror images to represent the free surface

3.1. Theory

The axial symmetrical formulation of Section 2.5 has many limitations if the effects of an underwater explosion near a 3-D floating structure are to be investigated as few realistic or interesting problems will have the required axial symmetry. Therefore, it is necessary to develop a fully 3-D version of the BIM method, which includes the effects of the

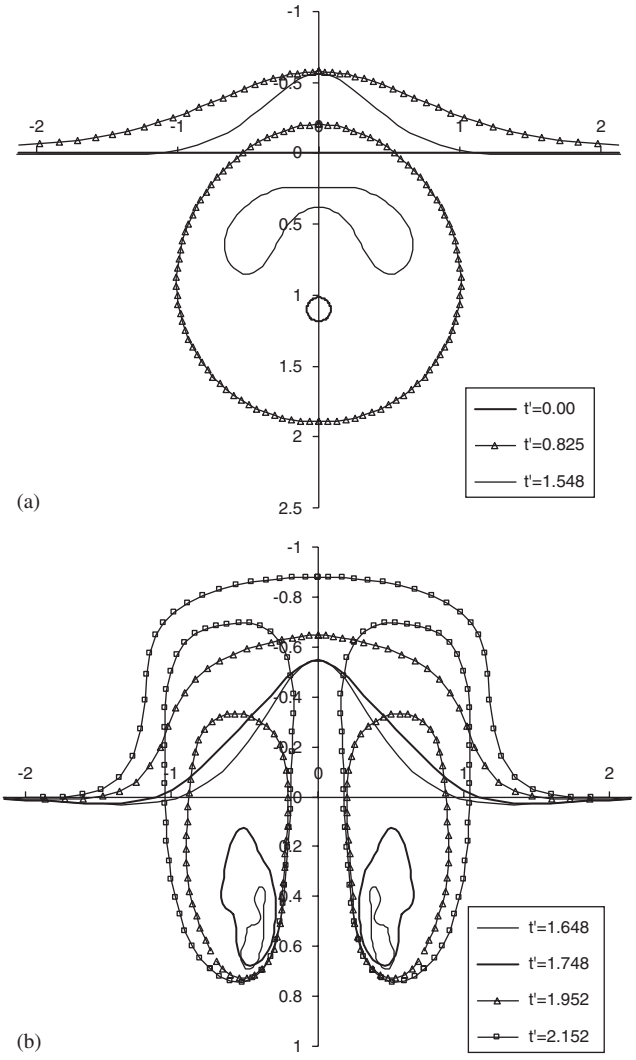

Fig. 2. As for Fig. 1, but with $\delta = 0.50$. The parameters are $\varepsilon = 500$ and $H' = 1.1$. (a) Bubble in its first expansion and collapse phase at $t' = 0.000$, $t' = 0.825$ and $t' = 1.548$. (b) Bubble in its second expansion phase at $t' = 1.648$, $t' = 1.748$, $t' = 1.952$ and $t' = 2.152$.

free surface. Three surfaces have to be taken into account: the bubble surface, the free surface and the submerged part of the hull of the floating structure or ship. Several problems arise in doing so. Firstly, the free surface needs very large meshing in a 3-D configuration and this will greatly increase numerical calculations. Secondly, the free surface is in contact with the structure. This not only can lead to numerical instabilities, but also a very complicated numerical procedure has to be enacted to follow the movement of the contact line between the ship and the free surface with some degree of robustness.

Several previous works have used the fact that the effect of a flat infinite solid fixed surface on an oscillating bubble at a certain distance away from the surface can be modelled by using the mirror image method [see Zhang et al. (2001), for example]. In these works, a (positive) image of the bubble is placed at the same distance behind the surface. In this way, the solid surface itself needs not be modelled explicitly. A similar approach can be adopted for the free surface in the 3-D computer code. The free surface, however, will act as a negative mirror. This approach will only be justified if the free surface remains relatively flat during the evolution of the bubble (i.e. if no significant plume is created on the free surface). A schematic picture of a typical ship structure is presented in Fig. 4(a). The parts of the ship above the waterline can be neglected in the current model. In Fig. 4(b) the ship and the explosion bubble and their images above the waterline are indicated. It seems advantageous in terms of numerical computation to divide the ship and its image

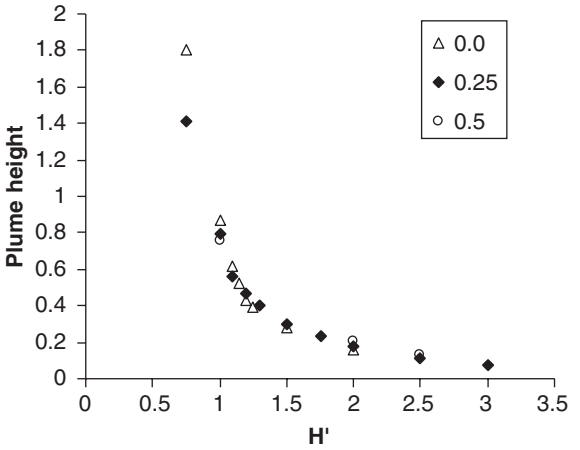

Fig. 3. The plume height as a function of the initial distance from the free surface H' for different values of $\delta = 0.0$, 0.25 and 0.5; $\varepsilon = 500$.

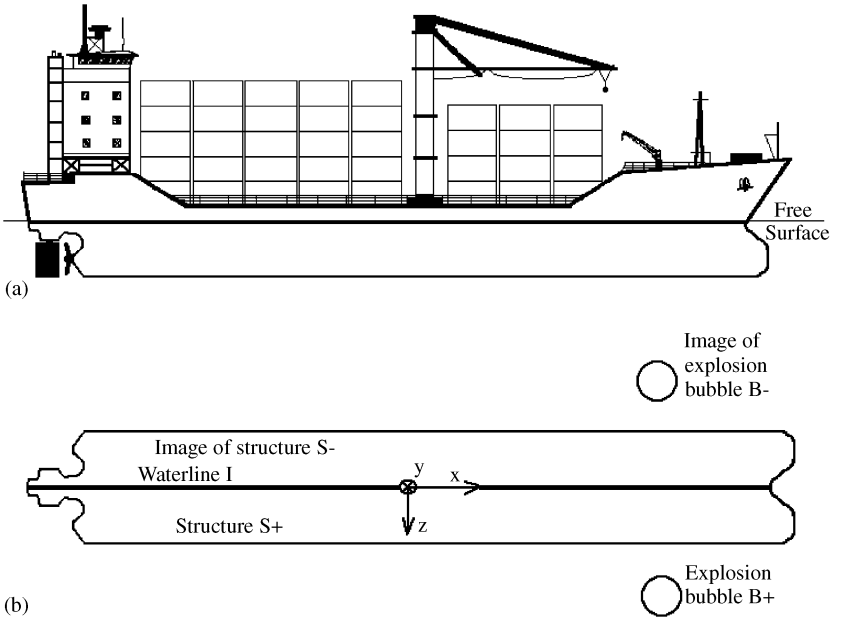

Fig. 4. (a) Picture of a typical ship. (b) Model of the submerged part of the ship S^+, the explosion bubble (B^+) and their images (S^- and B^-) above the water line I. The rudder and propeller have been removed for simplicity.

into three zones consisting of: nodes below the free surface (S^+), nodes on the free surface (I) and nodes above the free surface (S^-). The explosion bubble is indicated with B^+ and its image above the waterline with B^- in Fig. 4(b). The boundary integral equations can be written in this case as

$$c(\boldsymbol{y})\Phi(\boldsymbol{y}) + \int_{B^+ + B^- + S^+ + S^- + I} \Phi(x) \frac{\partial G(\boldsymbol{x}, \boldsymbol{y})}{\partial n} \mathrm{d}S = \int_{B^+ + B^- + S^+ + S^- + I} G(\boldsymbol{x}, \boldsymbol{y}) U(\boldsymbol{x}) \, \mathrm{d}S. \tag{23}$$

In this formulation, $\boldsymbol{y}$ is a fixed point and the integration variable $\boldsymbol{x}$ is located on the boundary of the problem. Eq. (23) relates the potential Φ and the normal velocity U. $c(\boldsymbol{y})$ corresponds to the solid angle when $\boldsymbol{y}$ is located on a boundary of the problem. The Green function or kernel, G, is defined as

$$\mathrm{G}(\boldsymbol{x}, \boldsymbol{y}) = \frac{1}{|\boldsymbol{x} - \boldsymbol{y}|}. \tag{24}$$

The integration in (23) is carried out over the surface of the bubble (B^+), its image (B^-), the submerged surface of the ship (S^+), its image above the waterline (S^-) and the contact line (or waterline: I). No meshing is required for the free surface. The surface of the bubble and the ship are discretized using triangular elements (the nodes corresponding to the corners of the triangle). A linear representation of the potential and the normal velocity is used. Integrating and storing the results for each node in vector notation (the $\mathbf{A}_S$ and $\mathbf{B}_S$ are matrices, while the Φ_S and U_S are vectors) transforms (23) to

$$\begin{bmatrix} \mathbf{A}_{S^+S^+} & \mathbf{A}_{S^+S^-} & \mathbf{A}_{S^+I} & \mathbf{A}_{S^+B^+} & \mathbf{A}_{S^+B^-} \\ \mathbf{A}_{S^-S^+} & \mathbf{A}_{S^-S^-} & \mathbf{A}_{S^-I} & \mathbf{A}_{S^-B^+} & \mathbf{A}_{S^-B^-} \\ \mathbf{A}_{IS^+} & \mathbf{A}_{IS^-} & \mathbf{A}_{II} & \mathbf{A}_{IB^+} & \mathbf{A}_{IB^-} \\ \mathbf{A}_{B^+S^+} & \mathbf{A}_{B^+S^-} & \mathbf{A}_{B^+I} & \mathbf{A}_{B^+B^+} & \mathbf{A}_{B^+B^-} \\ \mathbf{A}_{B^-S^+} & \mathbf{A}_{B^-S^-} & \mathbf{A}_{B^-I} & \mathbf{A}_{B^-B^+} & \mathbf{A}_{B^-B^-} \end{bmatrix} \bullet \begin{bmatrix} \boldsymbol{\Phi}_{S^+} \\ \boldsymbol{\Phi}_{S^-} \\ \boldsymbol{\Phi}_I \\ \boldsymbol{\Phi}_{B^+} \\ \boldsymbol{\Phi}_{B^-} \end{bmatrix}$$
$$= \begin{bmatrix} \mathbf{B}_{S^+S^+} & \mathbf{B}_{S^+S^-} & \mathbf{B}_{S^+I} & \mathbf{B}_{S^+B^+} & \mathbf{B}_{S^+B^-} \\ \mathbf{B}_{S^-S^+} & \mathbf{B}_{S^-S^-} & \mathbf{B}_{S^-I} & \mathbf{B}_{S^-B^+} & \mathbf{B}_{S^-B^-} \\ \mathbf{B}_{IS^+} & \mathbf{B}_{IS^-} & \mathbf{B}_{II} & \mathbf{B}_{IB^+} & \mathbf{B}_{IB^-} \\ \mathbf{B}_{B^+S^+} & \mathbf{B}_{B^+S^-} & \mathbf{B}_{B^+I} & \mathbf{B}_{B^+B^+} & \mathbf{B}_{B^+B^-} \\ \mathbf{B}_{B^-S^+} & \mathbf{B}_{B^-S^-} & \mathbf{B}_{B^-I} & \mathbf{B}_{B^-B^+} & \mathbf{B}_{B^-B^-} \end{bmatrix} \bullet \begin{bmatrix} \boldsymbol{U}_{S^+} \\ \boldsymbol{U}_{S^-} \\ \boldsymbol{U}_I \\ \boldsymbol{U}_{B^+} \\ \boldsymbol{U}_{B^-} \end{bmatrix}. \tag{25}$$

The geometry of this problem is symmetrical with respect to the waterline $z = 0$. Making use of this symmetry property and noting that all the matrices $\mathbf{A}$ and $\mathbf{B}$ are only dependant on this geometry (and not on the potential or the normal velocity), reveals that many matrices in the above equation are actually identical. So, $\mathbf{A}_{S^+S^+} = \mathbf{A}_{S^-S^-}$, $\mathbf{A}_{S^+S^-} = \mathbf{A}_{S^-S^+}$, $\mathbf{A}_{S^+I} = \mathbf{A}_{S^-I}$, $\mathbf{A}_{S^+B^+} = \mathbf{A}_{S^-B^-}$, $\mathbf{A}_{S^+B^-} = \mathbf{A}_{S^-B^+}$, $\mathbf{A}_{IS^+} = \mathbf{A}_{IS^-}$, $\mathbf{A}_{IB^+} = \mathbf{A}_{IB^-}$, $\mathbf{A}_{B^+S^+} = \mathbf{A}_{B^-S^-}$, $\mathbf{A}_{B^+S^-} = \mathbf{A}_{B^-S^+}$, $\mathbf{A}_{B^+I} = \mathbf{A}_{B^-I}$, $\mathbf{A}_{B^+B^+} = \mathbf{A}_{B^-B^-}$ and $\mathbf{A}_{B^+B^-} = \mathbf{A}_{B^-B^+}$. Similar relationships exist for the $\mathbf{B}$ matrices, for example:$\mathbf{B}_{B^+S^+} = \mathbf{B}_{B^-S^-}$ etc. The antisymmetric property of the potential problem leads to the following equalities: $\boldsymbol{\Phi}_{S^+} = -\boldsymbol{\Phi}_{S^-}$, $\boldsymbol{\Phi}_{B^+} = -\boldsymbol{\Phi}_{B^-}$, $\boldsymbol{\Phi}_I = 0$, $\boldsymbol{U}_{S^+} = -\boldsymbol{U}_{S^-}$, $\boldsymbol{U}_{B^+} = -\boldsymbol{U}_{B^-}$ and $\boldsymbol{U}_I = 0$. The third row of (25) gives the identity $0 = 0$. The first and second row and the fourth and fifth row of (25) are identical, respectively. Therefore, the whole system of equations can be reduced to

$$\begin{bmatrix} (\mathbf{A}_{S^+S^+} - \mathbf{A}_{S^+S^-}) & (\mathbf{A}_{S^+B^+} - \mathbf{A}_{S^+B^-}) \\ (\mathbf{A}_{B^+S^+} - \mathbf{A}_{B^+S^-}) & (\mathbf{A}_{B^+B^+} - \mathbf{A}_{B^+B^-}) \end{bmatrix} \bullet \begin{bmatrix} \boldsymbol{\Phi}_{S^+} \\ \boldsymbol{\Phi}_{B^+} \end{bmatrix}$$
$$= \begin{bmatrix} (\mathbf{B}_{S^+S^+} - \mathbf{B}_{S^+S^-}) & (\mathbf{B}_{S^+B^+} - \mathbf{B}_{S^+B^-}) \\ (\mathbf{B}_{B^+S^+} - \mathbf{B}_{B^+S^-}) & (\mathbf{B}_{B^+B^+} - \mathbf{B}_{B^+B^-}) \end{bmatrix} \bullet \begin{bmatrix} \boldsymbol{U}_{S^+} \\ \boldsymbol{U}_{B^+} \end{bmatrix}. \tag{26}$$

If the structure does not move, $\boldsymbol{U}_{S^+} = 0$. Bringing the unknown parameters to the left hand side and the known parameters to the right hand side, the final equation appears as

$$\begin{bmatrix} (\mathbf{A}_{S^+S^+} - \mathbf{A}_{S^+S^-}) & (-\mathbf{B}_{S^+B^+} + \mathbf{B}_{S^+B^-}) \\ (\mathbf{A}_{B^+S^+} - \mathbf{A}_{B^+S^-}) & (-\mathbf{B}_{B^+B^+} + \mathbf{B}_{B^+B^-}) \end{bmatrix} \bullet \begin{bmatrix} \boldsymbol{\Phi}_{S^+} \\ \boldsymbol{U}_{B^+} \end{bmatrix} = \begin{matrix} (-\mathbf{A}_{S^+B^+} + \mathbf{A}_{S^+B^-}) \bullet \boldsymbol{\Phi}_{B^+} \\ (-\mathbf{A}_{B^+B^+} + \mathbf{A}_{B^+B^-}) \bullet \boldsymbol{\Phi}_{B^+}. \end{matrix} \tag{27}$$

The diagonal terms of the matrices $\mathbf{A}_{S^+S^+}$ and $\mathbf{A}_{B^+B^+}$ can be obtained by taking 4π and subtracting the sum of all other terms in the same row for the same surface; see Taib (1985), Blake et al. (1987) or Liu and Rudolphi (2000). A further advantage is that there is no longer a need to calculate the solid angle $c(\boldsymbol{y})$. This procedure can only be performed for closed surfaces such as the bubble or the ship including its image. It may seem that there is no need to calculate the matrices $\mathbf{A}_{S^+I}$ and $\mathbf{A}_{B^+I}$, since these do not appear in (27). However, they are still needed in order to calculate the diagonal terms of the matrices $\mathbf{A}_{S^+S^+}$ and $\mathbf{A}_{B^+B^+}$. Similar results as obtained in (27) can probably be obtained by choosing a different Green function,

$$\mathrm{G}(\boldsymbol{x}, \boldsymbol{y}) = \frac{1}{|\boldsymbol{x} - \boldsymbol{y}|} - \frac{1}{|\boldsymbol{x} - \boldsymbol{y}_i|} \tag{28}$$

with $\boldsymbol{y}_i$ being the image point of $\boldsymbol{y}$, with respect to the $z = 0$ plane. However, the treatment of the singular terms of the matrix would be more cumbersome, since the surface of the ship would no longer be a closed surface and the 4π

procedure as described above would no longer be valid. The calculation of the strongest singularities would therefore have to be performed in a different way.

When the bubble enters its toroidal phase (after jet impact), a technique similar to the one described for the axial symmetrical configuration is applied. Details of this method can be found in Zhang et al. (2001). As in its axial symmetric counterpart a vortex ring is placed inside the bubble to take account of the circulation induced by the jet impact. The potential is again divided into a part originating from the vortex ring and a remainder. The assumption $\boldsymbol{U}_{S^+} = 0$ no longer applies in this situation; this velocity must now be assigned to a quantity equal but opposite to the velocity induced by the vortex ring on the structure. The equivalent of (27) will therefore be slightly more complicated.

As a further note, one should mention that a grid-redistribution scheme (called the Elastic Mesh Technique by Wang et al. 2003), has been applied at every time step on the bubble surface. This is done to avoid the nodes from clustering in one particular region, while leading to sparseness of nodes in other areas of the bubble. The Elastic Mesh Technique has also proven to be beneficial for the stability and speed of computation; previously nodes had to be added in the affected sparse areas, thus increasing the size of the problem and the time taken to solve for the corresponding new matrices increases.

It is important to investigate and ascertain when the above approximation with negative source images is valid and the effect on the accuracy of the calculations. In Fig. 3, the plume height as a function of H' is given for several values of δ. From Fig. 3 it is reckoned that for values of H' greater than 1.0, the error incurred becomes increasingly limited, if the free surface has been replaced by the above-described negative image method. In Section 3.2, it will be shown that the minimum distance where the employment of the 'negative mirror' for the free surface in the present 3D code is still feasible is $H' = 1.4$. The simulations to evaluate the flow physics of the bubble in the presence of a free surface and a floating structure are all carried out with a $H' > 1.5$ (see Section 4).

3.2. Comparison of the new model with the axial symmetrical model

It is important to test and verify the assembled 3-D code. It would be interesting to quantify the effect of the free surface on the bubble dynamics via the model employed in the 3-D code, as opposed to the axisymmetric code where the free surface is modelled explicitly. Unfortunately, no theoretical results are available to compare these results against. In order to do so, a bubble is initiated at a depth of $H' = 1.337$ with a strength of $\varepsilon = 395.7$ (incidently this corresponds to a TNT charge of 100 kg at a depth of 8.0 m). In this instance, gravity is neglected. The number of (3-D) nodes used on the bubble surface is 642 and the corresponding number of elements is 1280. The computed bubble shapes are shown in Fig. 5; Figs. 5(a)–(c) pertain to the 3-D simulation while Figs. 5(d)–(f) were calculated via the axisymmetrical code. The (imaginary) free surface is also indicated by a solid horizontal line in the 3-D simulations. For the 3-D simulations, the bubble starts as a spherical bubble ($t' = 0.000$), then grows rapidly before it reaches the maximum volume (Fig. 5(a)) at about $t' = 0.820$ (the corresponding dimensional bubble would have reached a radius of about 6.0 m). The bubble then starts contracting and at $t' = 1.468$ clearly a downwards directed jet develops in the upper part of the bubble (Fig. 5(b)). At $t' = 1.586$ a very peculiar flat jet develops (Fig. 5(c)). The bubble as a whole has moved downwards at the end of the simulation compared to the initial location. The results for a similar simulation with the axial symmetrical code (incorporating explicitly the free surface) are also given in Fig. 5(d)–(f). The bubble reaches its maximum volume at $t' = 0.860$ (Fig. 5(d)), this is very close to the value calculated for the 3-D code (0.820). At $t' = 1.626$, (Fig. 5(f)), the same peculiar jet shape is observed as in the 3-D simulation at $t' = 1.586$. The bubble also moves slightly downwards as for its 3-D counterpart. It may be noted, that the elevation of the free surface is still considerable (about 0.34) and is not quite negligible as yet. Even then, the bubble shapes are still reasonably similar between the two simulations. This provides the confidence that, even in these circumstances where the bubble is placed quite close to the free surface, the main physics of the bubble behaviour are still preserved.

Another example with similar parameters but with the bubble being placed deeper at $H' = 3.0$ was also considered (results not shown here). The jet tip was more rounded in this case. Both the 3-D and axial symmetrical results were very similar to those in the previous case. The times at which similar bubble shapes are observed correspond very well; a difference of less than 2% in time is found between the axisymmetric and 3-D simulations. The maximum elevation of the free surface is found to be 0.073 at $t' = 0.872$ (this corresponds well with Fig. 3). It should be mentioned that the gravity effect should be considered in an actual underwater explosion (though it may not be necessary for other simulations involving much smaller sized bubbles). Therefore, similar simulations but with the inclusion of the buoyancy parameter δ were also investigated. For example a simulation with $H' = 1.5$, $\delta = 0.30$ and the other parameters similar to those of Fig. 5, yielded an upwards jet for both the 3-D and axial symmetrical models (results not shown here) which impacted on the upper bubble surface at $t' = 1.658$ for the 3-D simulation and at $t' = 1.678$ for the axisymmetrical simulation. The maximum elevation of the free surface for the axisymmetrical code was 0.318 at

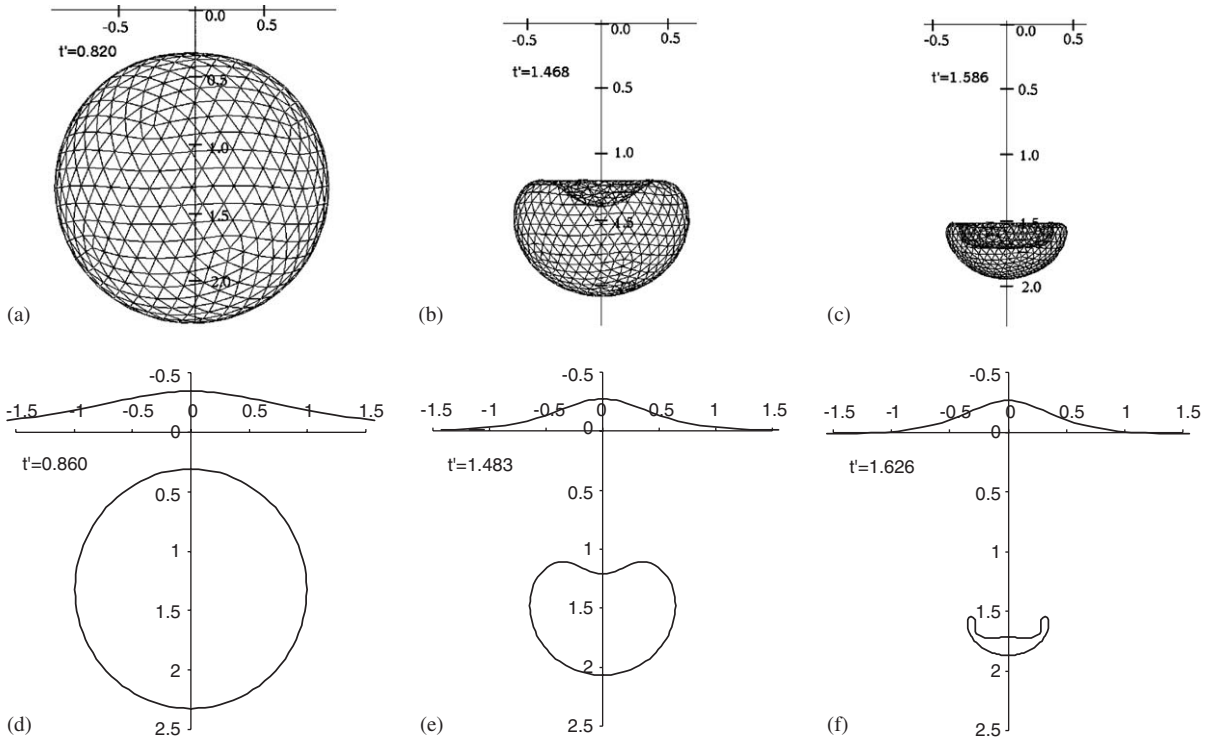

Fig. 5. Comparison of 3-D ((a)–(c)) and axially symmetric simulation ((d)–(f)) of a single bubble below a free surface with parameters $\varepsilon = 395.7$, $\delta = 0.0$ (no gravity) and $H' = 1.337$. The 3-D images ($t' = 0.820$, 1.468 and 1.586) are placed on top of their axisymmetric counterparts ($t' = 0.860$, 1.483 and 1.626).

$t' = 0.95$. Another test with $H' = 3.0$ and $\delta = 0.3$ also gave similar results for both the 3-D and axisymmetrical models (results not shown here). The maximum free surface elevation for the axisymmetrical code was 0.082 and was reached at $t' = 0.99$. Through the extensive tests in the above-mentioned cases and others, and comparing the results of the 3-D code with the results obtained with the axisymmetrical code, it is believed that the assembled 3-D code using the negative image method is describing reasonably well the true dynamics of a bubble.

Another feature worth noting is that from Fig. 5, had a smaller H' like say 1.3 being considered, the bubble would have expanded beyond the $z = 0$ axis at the first maximum volume (thus intersecting with its own image and hence leading to numerical problems and/or incorrect results). Therefore, conservatively we have stated that a minimum $H' = 1.4$ should be imposed for the present 'negative' image method in the 3-D code to work reasonably well and accurately.

There is no upper limit for H', though the influence of the free surface becomes negligible for very large values of H' (>20). In that case there will no longer be a free surface induced downwards jet. Either gravity will produce a jet or the bubble will remain spherically symmetric (for small values of δ).

4. Bubble dynamics near free surface and floating structure

In this section, the negative image model incorporated in the 3-D code is used to simulate the behaviour of an explosion bubble in the vicinity of both a free surface and a ship. The developed framework with the 'negative' image method can handle flexible and/or mobile structures. However, the ship in this work is assumed to be rigid and immobile. In Fig. 6 the mesh of a ship is shown as it is used in the subsequent simulations. In Fig. 6(a) the total ship is shown (front and back view). The part that is submerged under water (the mesh above the waterline is neglected as shown in Fig. 6(b)) has 3199 nodes and 6240 triangular elements. The ship has a length of almost 100 m as it stretches from $x = 53.0$ (front of the ship) to $x = -51.1$ m (back of the ship). The plane $y = 0$ is a plane of symmetry coinciding

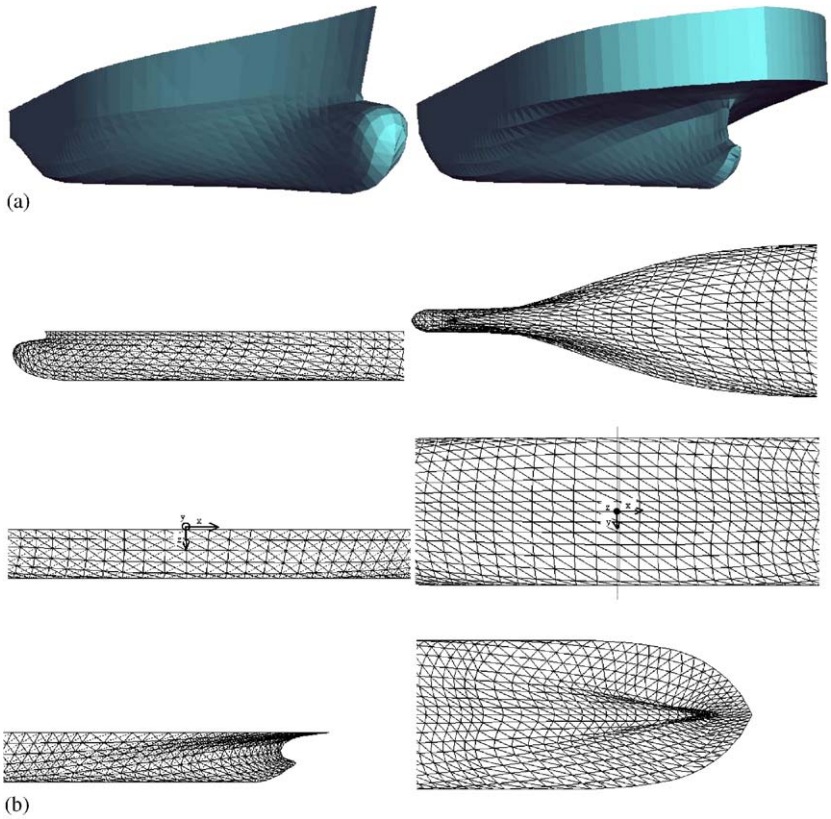

Fig. 6. (a) Front and back view of the mesh of the submerged portion of a typical ship for use in the numerical calculations. (b) Side views and top view of the ship model; front, middle and back section. The free surface is located at the top of the ship model ($z = 0$).

with the centreline of the ship. The largest width of the ship is 14.0 m (from $y = -7.0$ to $y = 7.0$). The intersection of $z = 0.0$ m and the ship is located at the waterline. The bottom of the ship is situated at $z = 4.70$ m.

In Case 1, an initial bubble based on an explosive charge of 100 kg is placed exactly below the centre of the ship (see Fig. 7(a) and Fig. 7(g)) at a depth of 12.0 m. The maximum bubble radius is $R_m = 5.60$ m at this depth. The dimensionless stand-off distance (i.e. the smallest distance between the ship and the explosive) is 1.30. The other dimensionless parameters are $\varepsilon = 334.9$, $H' = 2.14$ and $\delta = 0.251$. The initial bubble resulting from the explosion can be observed in Fig. 7(a). The maximum bubble size occurs at $t' = 0.965$; in Fig. 7(b) the bubble shape is depicted near this time at $t' = 0.917$. The bubble grows very fast initially, but stays for a relatively long time in the near-maximum size. An upwards directed jet is developing, as can be observed in Fig. 7(c) ($t' = 1.801$). The jet impacts on the upper part of the bubble surface at $t' = 1.820$. In Fig. 7(d), the resulting toroidal bubble shape is shown at $t' = 1.843$. A vortex ring has been placed in the interior of the bubble and it is depicted as a thick bar in the same Fig. 7(d). Next, the bubble continues to contract in volume until it reaches its minimum at $t' = 2.094$. In Fig. 7(e), the shape of the bubble near this minimum volume is shown. It assumes a kind of 'mushroom' shape. After reaching its minimum volume (which is larger than the volume at $t' = 0$ due to energy considerations), the bubble starts its second expansion phase as shown in Fig. 7(f). The bubble has moved upwards during the whole process and is almost touching the ship's bottom at the end of the simulation. In Fig. 7, the dimensional times are also indicated for reference purposes; Fig. 7(f) corresponds to a dimensional time of $t = 0.84$ s.

The next case, Case 2, is given in Fig. 8. The same charge of 100 kg TNT is now placed at a location of 8.0 m besides the same immobile ship. The bubble is deliberately placed nearer to the free surface at a depth of 9.0 m, in order to see the effects of the free surface on the bubble dynamics. The x-location of the explosive is not changed (i.e. Fig. 7(g) is still valid). The dimensionless parameters are: $\varepsilon = 378.3$, $H' = 1.53$ and $\delta = 0.304$. These parameters are slightly different from those presented in Fig. 7. The maximum bubble radius is almost similar to the previous Case 1 and is $R_m = 5.88$ m. The effects of the free surface are expected to be larger in this case, because of the closer proximity. The bubble starts growing very rapidly again and reaches its maximum size at $t' = 0.912$ as depicted in Fig. 8(b). The stand off distance is

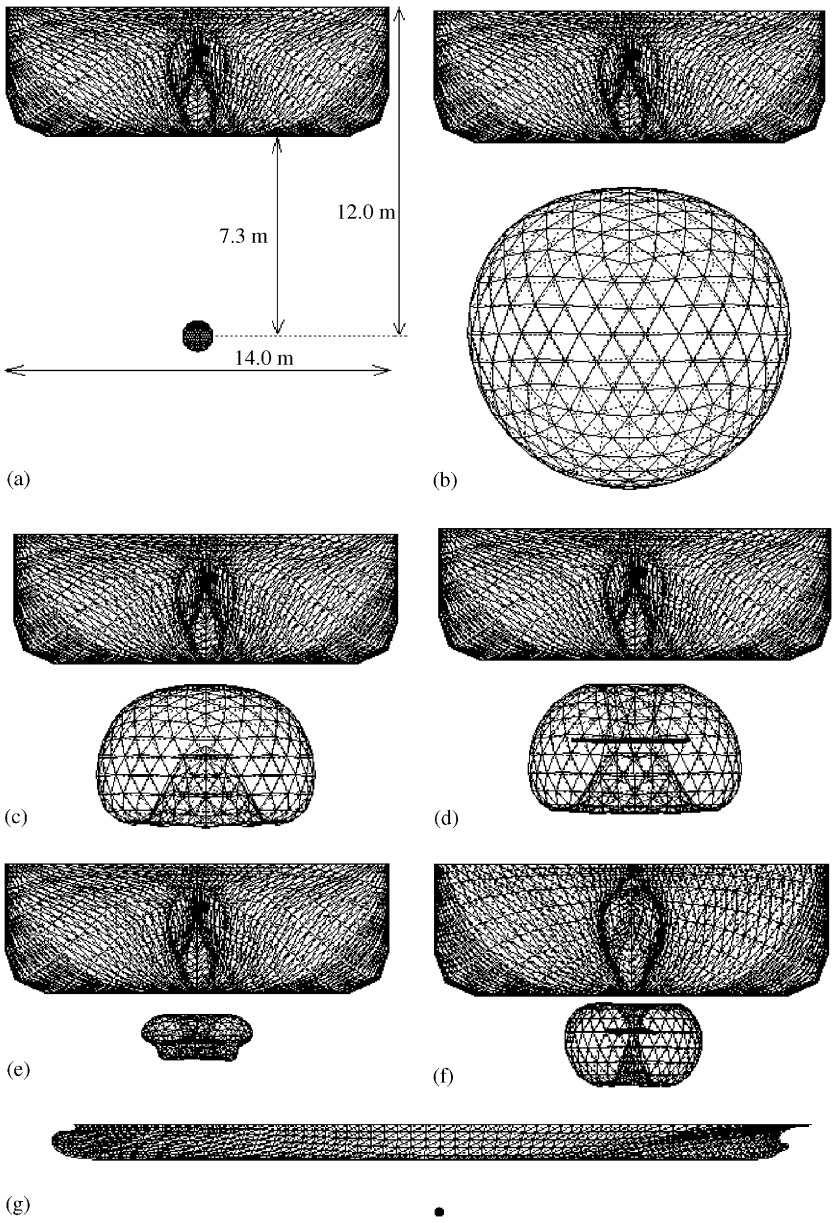

Fig. 7. Case 1: Behaviour of an explosion bubble near a ship (front view, explosive equivalent to 100 kg TNT placed 12.0 m below free surface, exactly underneath ship). The dimensionless parameters are $\varepsilon = 334.9$, $H' = 2.14$ and $\delta = 0.251$. Bubble shapes at (a) $t' = 0.0$ or $t = 0.0$ s, (b) $t' = 0.917$ or $t = 0.35$ s, (c) $t' = 1.801$ or $t = 0.68$ s, (d) $t' = 1.843$ or $t = 0.70$ s, (e) $t' = 2.052$ or $t = 0.78$ s, (f) $t' = 2.218$ or $t = 0.84$ s and (g) side view at $t' = 0.0$.

smaller than the previous Case 1 and the bubble can be seen to wrap around the hull of the ship. Numerical instabilities can occur when the nodes of the ship and the bubble approach each other too closely. Therefore, the bubble is not allowed to expand too near to the surface of the ship. The minimum dimensionless distance the bubble is allowed to approach the surface is set at 0.05. It is found that the overall dynamics and behaviour of the bubble is not very sensitive to the exact value of this minimum distance (not shown). Following the work of Rungsiyaphornrat et al. (2003), a check on the associated Reynolds number based on a typical velocity in the gap and the minimum distance for the gap size reveals a quantity always much larger than $\mathcal{O}(1)$. This implies that viscous effects, if any, are completely overshadowed by the inertial effects pertaining to the underwater explosion simulations under consideration. In Fig. 8(c), a jet originating from the bottom part of the bubble can be seen to start developing. However, at the same time an

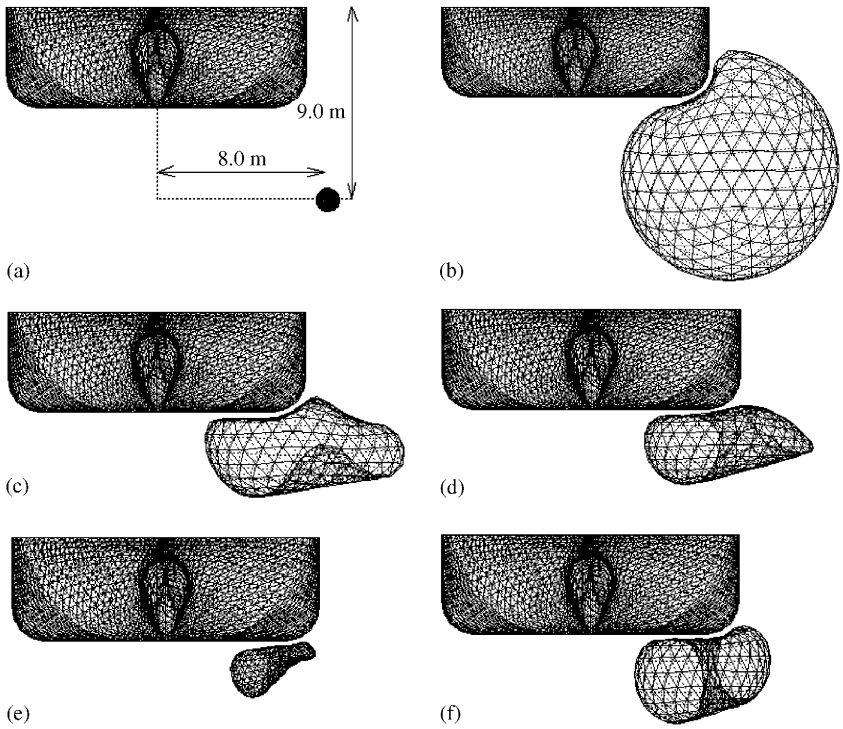

Fig. 8. Case 2: Behaviour of an explosion bubble near a ship (front view, explosive equivalent to 100 kg TNT placed at 9.0 m below the free surface and 8.0 m besides the axis of symmetry of the ship). The dimensionless parameters are: $\varepsilon = 378.3$, $H' = 1.53$ and $\delta = 0.304$. Bubble shapes at (a) $t' = 0.0$ or $t = 0.0$ s, (b) $t' = 0.63$ or $t = 0.27$ s, (c) $t' = 1.674$ or $t = 0.72$ s, (d) $t' = 1.708$ or $t = 0.73$ s, (e) $t' = 1.90$ or $t = 0.82$ s, (f) $t' = 2.37$ or $t = 1.02$ s.

indentation occurs at the upper part of the bubble away from the free surface. The jet in the lower part is largely due to the effect of gravity. The indentation on top of the bubble is the beginning of a downwards directed jet induced by the free surface. This latter jet does not develop completely, since the upwards directed jet impacts earlier on the upper part of the bubble surface near the ship (Fig. 8(d)) and a toroidal bubble is being created. At $t' = 1.90$, the bubble reaches its smallest volume (Fig. 8(e)). At the same time, the bubble's centre of gravity has moved towards the ship due to the attraction of a bubble towards a solid structure and the influence of buoyancy. In Fig. 8(f) the bubble has started to grow again. The series of events in Fig. 8 indicate that a very complex interaction exists for the bubble dynamics as it is affected by gravity, the repulsion of the free surface and the attraction towards the structure. The bubble reaches its minimum volume earlier than in the previous Case 1 ($t' = 1.90$ versus $t' = 2.05$, respectively); this is possibly due to the closer proximity of the free surface. Again, the dimensional times are also indicated for reference purposes.

From a flow physics point of view, an even more interesting Case 3 is shown in Fig. 9. In Case 3, the explosion bubble is again placed at a depth of 9.0 m, but at an even larger horizontal distance from axis of the ship at 15.0 m (see Fig. 9(a)). The stand-off distance is now comparable to Case 1. The dimensionless parameters are $\varepsilon = 378.3$, $H' = 1.53$ and $\delta = 0.304$ (similar to Case 2). The influence of the attraction of the ship is expected to be less in this case. The maximum volume of the bubble is reached at a dimensionless time of $t' = 0.883$; this is earlier than in Cases 1 and 2 (probably because the influence of the free surface is even greater in this case). The bubble is still more or less spherical at this instance (see Fig. 9(b)). An upwards directed jet develops (Fig. 9(c)) at the bottom of the bubble. At the same time the upper part of the bubble starts moving downwards slightly (this is interpreted as the beginning of a downwards jet). However, as in Case 2, the upwards jet impacts on the upper bubble surface before the downwards free-surface induced jet has the opportunity to develop further. The resulting toroidal bubble of Fig. 9(d) looks fairly symmetrical, since the gravity jet is directed almost straight upwards (with the influence of the presence of the ship weaker on comparing to Case 2). This symmetry is quickly lost and the right portion of the bubble becomes smaller and smaller compared to the left portion (Fig. 9(e)). The bubble reaches its minimum volume at $t' = 1.738$ and starts growing again (Fig. 9(f)). During this stage, a very interesting phenomenon can be observed. This is best seen by zooming in on the bubble just after the jet impact at times ranging from $t' = 1.729$ to $t' = 1.775$ as shown in Fig. 10. Very soon after the jet

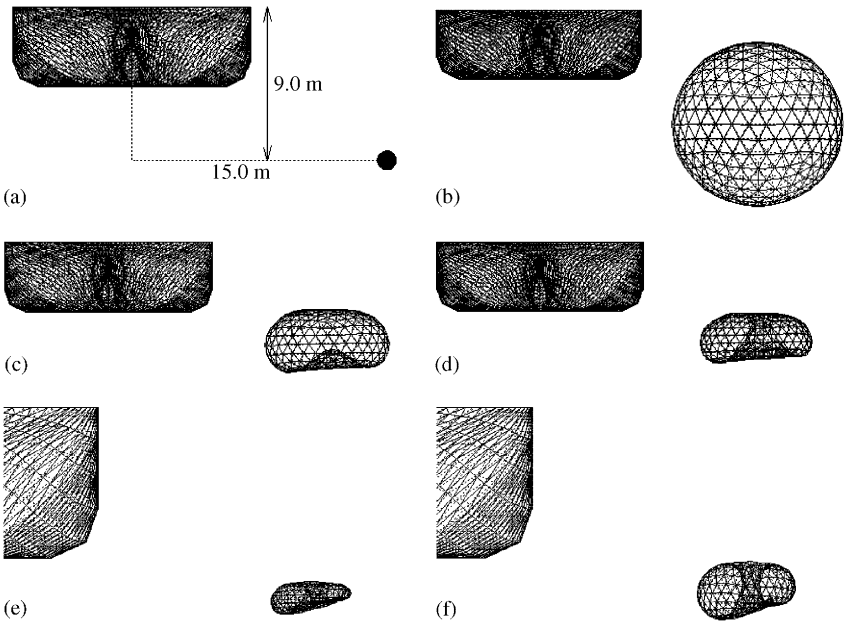

Fig. 9. Case 3: Behaviour of an explosion bubble near a ship (front view, explosive equivalent to 100 kg TNT placed at 9.0 m below the free surface and 15.0 m besides the axis of symmetry of the ship). The dimensionless parameters are the same as in Case 2. Bubble shapes at (a) $t' = 0.0$ or $t = 0.0$ s, (b) maximum volume; $t' = 0.875$ or $t = 0.38$ s, (c) $t' = 1.59$ or $t = 0.69$ s, (d) $t' = 1.643$ or $t = 0.71$ s; (e) zoom-in of the minimum volume at $t' = 1.738$ or $t = 0.75$ s, (f) zoom-in at $t' = 1.759$ or $t = 0.758$ s.

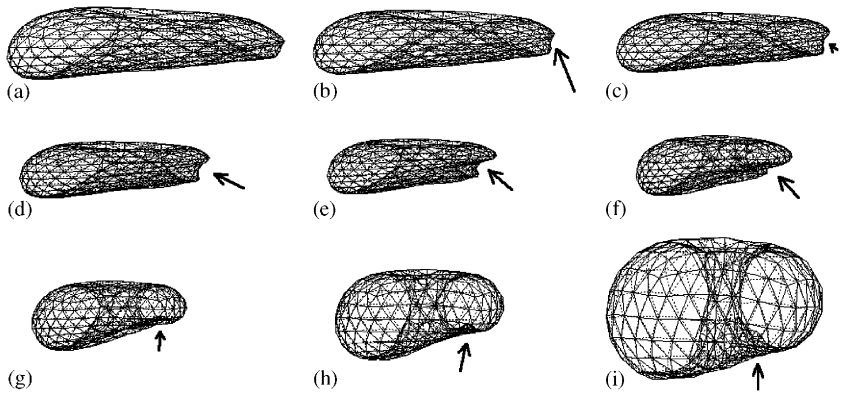

Fig. 10. Case 3: Close-up view of the turning secondary 'jet' just after jet impact from $t' = 1.729$ to $t' = 1.775$ (corresponds to dimensional times between $t = 0.738$ s and $t = 0.758$ s). Bubble shapes at: (a) $t' = 1.729$, (b) $t' = 1.733$, (c) $t' = 1.736$, (d) $t' = 1.739$, (e) $t' = 1.743$, (f) $t' = 1.748$, (g) $t' = 1.753$, (h) $t' = 1.759$; also corresponding to Fig. 9(f) and (i) $t' = 1.775$.

impact, the bubble assumes a very flat shape as in Fig. 10(a). As noted, the right portion of the bubble contracts much more rapidly than the left portion. At the same time, the bubble topology shows that an indentation on the bubble surface of the right portion can be observed. This is indicated with an arrow in Fig. 10(b). This indentation may serve as the beginning of the formation of another (secondary) jet; it is initially directed towards the ship. However, the first upwards directed jet due to buoyancy still has a very large influence on the flow field. The liquid in the lower neighbourhood of the bubble is transported through the centre of the toroidal bubble towards the region above the bubble. The indentation also moves towards the centre of the toroidal bubble (Figs. 10(d)–(f)). In Figs. 10(g) and (h) the indentation has moved from the right portion to the bottom portion of the bubble. At about this time the bubble has reached its minimum volume and starts growing again. As the bubble grows further (Fig. 10(i)), this secondary 'jet' has

almost completely disappeared. The sequence of events described is interpreted as the beginning of the formation of a jet towards the ship; however, this 'rotating jet' is transported by the main flow and does not have enough momentum to develop further. Nevertheless, the bubble as a whole has been moved considerably towards the structure in this short period of time. Case 3 shows very clearly the complex interactions that can occur during the oscillation of a bubble near a structure and a free surface in the presence of buoyancy effects.

Another example (Case 4) is given in Fig. 11. The same explosive charge of 100 kg is now positioned at the front of the ship at $x = 54.0$, $y = 0.0$, $z = 9.0$ m. The dimensionless parameters are the same as in Case 2. In Fig. 11(a) the initial bubble is shown. At $t' = 0.861$ the bubble reaches its maximum shape and wraps around the front part of the ship. In Fig. 11(c) an upwards directed jet can be seen to develop originating from the bottom of the bubble, an indentation of the top part can also be observed (due to the influence of the free surface). At $t' = 1.663$ the jet impacts obliquely, directed towards the front part of the ship. In Figs. 11(e) and (f) the bubble has reached its toroidal shape. It shrinks further and at the same time moves further below the ship. In Fig. 11(f) a strange lobe can be seen at the left bottom part of the bubble. A zoom-in is given in Fig. 11(h). This lobe could be interpreted as the formation of a second jet. However, this jet does not develop further and the lobe disappears after the bubble has reached its minimum volume and starts growing again (Fig. 11(g)). In Case 4, the bubble is clearly attracted towards the ship (compare Fig. 11(a) with (g)). Other simulations with similar bubbles located at $x = 56$ m and $x = 58$ m (as in Case 4, keeping the other parameters the same, results not shown here) have been performed. In those cases, the charge is located too far from the ship and the bubble exhibits a behaviour very similar to a similar bubble near a free surface without the presence of a ship.

Finally, it may be mentioned that the pressure on the hull of the ship has been calculated (not shown here). As expected, the pressure approaches the atmospheric pressure when z approaches 0. The pressure on the hull just after the explosion is highest at the location closest to the explosive charge. When the bubble reaches its maximum size, the pressure becomes much less then the atmospheric pressure (as well as the pressure inside the bubble). The jet impact generates another pressure peak near the region of the jet impact. The results are not depicted here, since this article is mainly dealing with the dynamics of the bubble and less with the influence of the explosion on the ship.

5. Discussion and conclusion

As shown above, the behaviour of a bubble in the vicinity of both a fixed solid structure and a free surface can be quite complicated. This is even more so, when gravity effects are nonnegligible. A "new model" was developed based on the fact that the free surface can be interpreted as a negative mirror under certain circumstances. This is only valid when the free surface remains relatively flat during the evolution of the bubble. In that case the free surface no longer needs to be modelled explicitly. Several tests have been performed to ensure that the new model gives comparable results to those obtained from a previous axially symmetric model. In the examples shown, all three effects; i.e. proximity to the solid surface, proximity to the free surface and buoyancy, play their respective important roles. A bubble placed at 'large' distances from the free surface and the structure will only exhibit an upwards jet due to gravity. The distance can be considered 'large' for dimensionless depths greater then $H' = 2.0$ for the case under investigation with relatively large values of δ ($\delta \sim 0.3$). Bubbles placed near a free surface, but without a solid structure were also considered. An excellent agreement with the results of an existing axial symmetrical code was obtained (the latter having taken into consideration both the movement and interaction of the bubble with the free surface). The lower limit of H' that can be used with the new model is $H' = 1.4$. Taking smaller values of H' may result in the bubble and its image crossing each other, which in turn will lead to numerical failure. For cases of H' smaller than 1.4 the present negative image model should be replaced with a model that takes into account the movement of the free surface. There are no limits for the maximum depth of H' in the current model, though it is expected that for very large H' (>20) the free surface will hardly have any influence on the dynamics of the bubble.

A bubble placed near a ship will, in many cases, develop a jet directed towards this ship. This jet can be very powerful and is capable of destroying the ship (typical jet velocities can be 100 m/s or larger). Depending on the exact location of the bubble, the proximity to the free surface and the influence of gravity, the jet may impact on the structure or miss it completely. Therefore a thorough knowledge of the bubble dynamics can mean the difference between the survival or destruction of a ship.

It might be noted here that the theoretical framework developed is not limited to applications associated with underwater explosions. Though the discussions in this article are limited to that particular area, the same framework can also be used to simulate much smaller bubbles (in that case the influence of buoyancy will be greatly reduced).

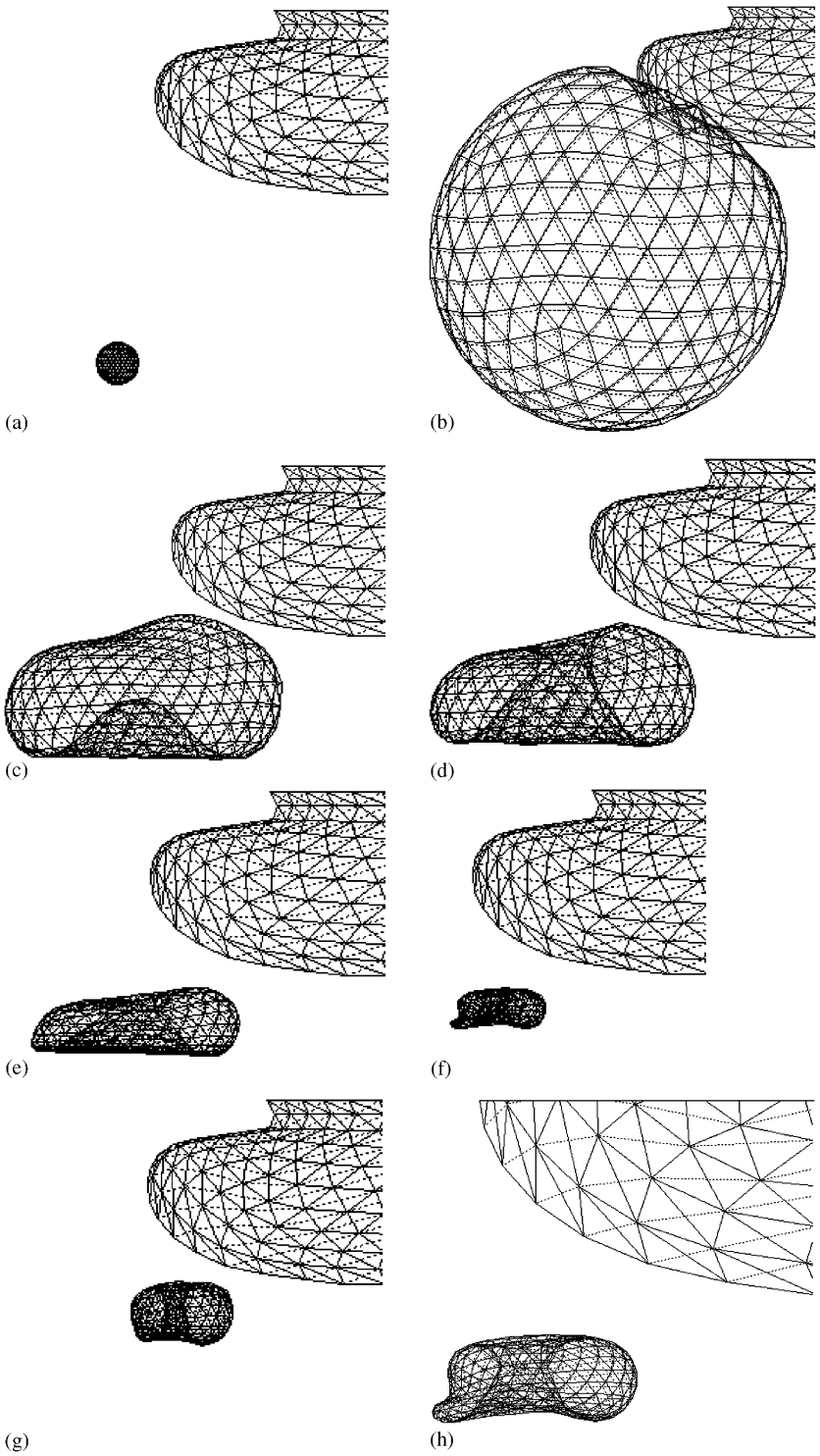

Fig. 11. Case 4: Behaviour of an explosion bubble near a ship (side view, explosive equivalent to 100 kg TNT placed at $x = 54.0$, $y = 0.0$, $z = 9.0$ m). The dimensionless parameters are the same as in Case 2. Bubble shapes at (a) $t' = 0.0$ or $t = 0.0$ s, (b) maximum volume; $t' = 0.861$ or $t = 0.368$ s, (c) $t' = 1.630$ or $t = 0.694$ s, (d) jet impact at $t' = 1.663$ or $t = 0.710$ s, (e) $t' = 1.707$ or $t = 0.729$ s, (f) around the minimum volume $t' = 1.740$ or $t = 0.743$ s, (g) $t' = 1.754$ or $t = 0.749$ s; (h) a zoom-in of (f).

References

Benjamin, T.B., Ellis, A.T., 1966. Cavitation: the collapse of cavitation bubbles and the pressures thereby produced against solid boundaries. Philosophical Transactions of the Royal Society of London 260, 221–240.

Blake, J.R., Gibson, D.C., 1981. Growth and collapse of a vapour cavity near a free surface. Journal of Fluid Mechanics 111, 123–140.

Blake, J.R., Gibson, D.C., 1987. Cavitation bubbles near boundaries. Annual Review of Fluid Mechanics 19, 99–123.

Blake, J.R., Taib, B.B., Doherty, G., 1986. Transient cavities near boundaries. Part 1. Rigid boundary. Journal of Fluid Mechanics 170, 479–497.

Blake, J.R., Taib, B.B., Doherty, G., 1987. Transient cavities near boundaries. Part 2. Free surface. Journal of Fluid Mechanics 181, 197–212.

Blake, J.R., Hooton, M.C., Robinson, P.B., Tong, R.P., 1997. Collapsing cavities, toroidal bubbles and jet impact. Philosophical Transactions of the Royal Society of London A 355, 537–550.

Chahine, G.L., 1977. Interaction between an oscillating bubble and a free surface. Journal of Fluids Engineering. Series I 99, 709–716.

Chahine, G.L., 1994. Strong interactions bubble/bubble and bubble/flow. Bubble Dynamics and Interface Phenomena. Kluwer Academic Publishers, Dordrecht, pp.195–206.

Chan, P.C., Kan, K.K., Stuhmiller, J.M., 2000. A computational study of bubble-structure interaction. Journal of Fluids Engineering 122, 783–790.

Cole, R.H., 1948. Underwater Explosions. Princeton University Press, Princeton, pp. 270–352.

Harris, P.J., 1992. A numerical model for determining the motion of a bubble close to a fixed rigid structure in a fluid. International Journal for Numerical Methods in Engineering 33, 1813–1822.

Klaseboer, E., Khoo, B.C., 2004. Boundary integral equations as applied to an oscillating bubble near a fluid-fluid interface. Computational Mechanics 33, 129–138.

Liu, Y.J., Rudolphi, T.J., 2000. New identities for fundamental solutions and their applications to non-singular boundary element formulations. Computational Mechanics 24, 789–795.

Longuet-Higgins, M.S., 1983. Bubbles, breaking waves and hyperbolic jets at a free surface. Journal of Fluid Mechanics 127, 103–121.

Naude, C.F., Ellis, A.T., 1961. On the mechanism of cavitation damage by non-hemispherical cavities in contact with a solid boundary. ASME Journal of Basic Engineering 83, 648–656.

Plesset, M.S., Chapman, R.B., 1971. Collapse of an initially spherical vapor cavity in the neighborhood of a solid boundary. Journal of Fluid Mechanics 47, 283–290.

Prosperetti, A., 2004. Bubbles. Physics of Fluids 16 (6), 1852–1865.

Rayleigh, L., 1917. Philosophical Magazine 34, 94–98.

Robinson, P.B., Blake, J.R., Kodama, T., Shima, A., Tomita, Y., 2001. Interaction of cavitation bubbles with a free surface. Journal of Applied Physics 89 (12), 8225–8237.

Rungsiyaphornrat, S., Klaseboer, E., Khoo, B.C., Yeo, K.S., 2003. The merging of two gaseous bubbles with an application to underwater explosions. Computers & Fluids 32, 1049–1074.

Taib, B.B., 1985. Boundary integral methods applied to cavitation bubble dynamics. Ph.D. Thesis, University of Wollongong.

Wang, C., Khoo, B.C., Yeo, K.S., 2003. Elastic mesh technique for 3D BIM simulation with an application to underwater explosion bubbles. Computers and Fluids 32 (9), 1195–1212.

Wang, Q.X., Yeo, K.S., Khoo, B.C., Lam, K.Y., 1996a. Strong interaction between a buyoancy bubble and a free surface. Theoretical and Computational Fluid Dynamics 8, 73–88.

Wang, Q.X., Yeo, K.S., Khoo, B.C., Lam, K.Y., 1996b. Nonlinear interaction between gas bubble and free surface. Computers & Fluids 25 (7), 607–628.

Zhang, S., Duncan, J.H., 1994. On the nonspherical collapse and rebound of a cavitation bubble. Physics of Fluids 6 (7), 2352–2362.

Zhang, Y.L., Yeo, K.S., Khoo, B.C., Chong, W.K., 1998. Three-dimensional computation of bubbles near a free surface. Journal of Computational Physics 146, 105–123.

Zhang, Y.L., Yeo, K.S., Khoo, B.C., Wang, C., 2001. 3D Jet impact and toroidal bubbles. Journal of Computational Physics 166, 336–360.